CHEMISTRY OF MATERIALS

Article

pubs.acs.org/cm

Enhancement of Acid Photogeneration Through a Para-to-Meta Substitution Strategy in a Sulfonium-Based Alkoxystilbene Designed for Two-Photon Polymerization

Rongjie Xia,[†] Jean-Pierre Malval,*[,‡] Ming Jin,*[,†] Arnaud Spangenberg,[‡] Decheng Wan,[†] Hongting Pu,[†] Thomas Vergote,[‡,§] Fabrice Morlet-Savary,[‡] Hélène Chaumeil,[§] Patrice Baldeck,[∥] Olivier Poizat,[⊥] and Olivier Soppera[‡]

[†]Institute of Functional Polymer Materials, Tongji University, 1239 Siping Road, 200092 Shanghai, China

[‡]Institut de Sciences des Matériaux de Mulhouse, LRC CNRS 7228, Université de Haute Alsace, 15 Rue Jean Starcky, 68057 Mulhouse, France

[§]Laboratoire de Chimie Organique et Bioorganique EA 4566, Université de Haute Alsace, ENSCMu, 3 Rue Alfred Werner, 68093 Mulhouse, France

[∥]Laboratoire Interdisciplinaire de Physique, UMR CNRS 5588, Université Joseph Fourier, 38402 Saint Martin d'Hères, France

[⊥]Laboratoire de Spectrochimie Infrarouge et Raman, UMR CNRS 8516, Université des Sciences et Technologies de Lille, 59655 Villeneuve d'Ascq Cedex, France

Supporting Information

ABSTRACT: This contribution reports on the synthesis and the photochemical behavior of two new sulfonium-based photoacid generators (PAGs). We demonstrate that a para-to-meta substitution of a methyl (*p*-cyanobenzyl) sulfonium group in a 4-alkoxystilbene core strongly influences the photodissociation efficiency of the PAGs and leads to an increase of the quantum yield for acid generation by a factor 2.4. This substantial effect, which was also corroborated by a reactivity enhancement in cationic photopolymerization, is assigned to the modulation of the electronic interaction between two low lying excited states whose energy gap is strongly influenced by this substitution effect. Moreover, it was found that the position of the sulfonium moiety hardly affects the two-photon absorption properties of these push−pull chromophores. By the two-photon fabrication of microstructures, we finally show the potential use of the meta derivative as cationic two-photon initiator.

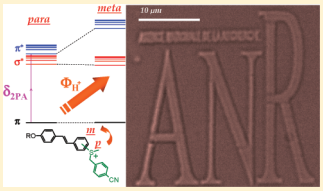

KEYWORDS: *two-photon absorption, photoacid generators, microfabrication*

1. INTRODUCTION

Photoacid generators (PAGs) constitute an important class of cationic photoinitiators that occupy a strategic position in the field of the photoresists.[1,2] The applications of PAGs have been extensively developed in various research domains such as microelectronics,[3] photosensitized resins,[4−6] 3D microfabrication, and high density optical data storage.[7] Commercial PAGs are mainly photoactivated through direct excitation at wavelengths ranging from VUV to close-UV.[3,8−14] This irradiation mode enables to reach submicrometric resolutions, according to the Rayleigh diffraction limit. However, because of the nonselective excitation of the photoinitiator, undesirable side reactions consecutive to the excitation of PAGs byproduct should also occur.[1,2,5,10] Moreover, a severe restriction in the choice of the resin can be necessary as a result of the bulk inner filter, which thus hampers the extension to new applications such as the 3D-microfabrication. To achieve the specific excitation of the PAGs with a concomitant improvement of spatial resolution, the two-photon activation process constitutes an alternative solution.[4,7,15−19] In this case, two approaches are mainly adopted. The first one, which is derived from one-photon sensitizing methods,[20−22] consists of associating a two-photon active sensitizer, such as coumarin,[23] phenothiazine,[24] or thioxanthone,[25] with a commercial PAG, such as onium salts. The acid generation generally proceeds through a photo-induced electron transfer (PET) from the excited sensitizer to the PAG. However, the global kinetics of this bimolecular method is intrinsically limited by diffusion. Therefore, an integrated approach can be alternatively proposed.[25−29] It is based on the molecular association of the acid generator functionality into the structure of the two-photon active chromophore. This appealing strategy has been nicely exemplified by Perry et al.,[26−28] who designed a sulfonium-based bis[(diarylamino)styryl]benzene derivative that exhibits both high quantum yield for acid generation (∼ 0.5) and large two-photon absorption (2PA) cross sections (δ). It should be noted that in this D−π−D system, the dimethylsulfonium substituents were localized in the meta position, with respect to the amino groups. More recently, Belfield et al.[29] developed a 1,8-bis(4′-styryl)fluorene with two para-substituted diphenyl-

Received: February 27, 2011
Revised: December 14, 2011
Published: December 14, 2011

sulfonium groups at both extremities of the PAGs. Even if this molecular architecture is similar to the previous one (i.e., A−π−A) and the exergonic character of the intramolecular PET is assumed, the quantum yield for acid generation drops to a value 6 times lower. This dramatic decrease in acid generation efficiency should be first ascribed to the leaving-group propensity of the substituents on the sulfonium subunit. Indeed, Sullivan et al.[30] showed that a methyl group cleaved more easily than a phenyl one. Moreover, as a result of the extension of electronic conjugation, the positioning of the sulfonium substituent should influence the acid generation efficiency as well as the two-photon absorption cross section. To our knowledge, such combined effect has not been clearly rationalized, even if it could open up some relevant routes for the design of highly sensitive two-photon activable PAGs. In this context, we investigate herein the photochemical behavior of a 4-ethoxystilbene derivative in which a methyl(*p*-cyanobenzyl)sulfonium is substituted in either the 4′ position (**EtO-PS**) or the 3′ position (**EtO-MS**) (see Scheme 1). The *p*-cyanobenzyl moiety was chosen because of its better leaving propensity as the methyl group.[30,31] Linear and nonlinear spectroscopic analyses of these new PAGs are presented in close connection with their reactivity in one- and two-photon cationic photopolymerization.

Scheme 1. Molecular structures of EtO-PS and EtO-MS

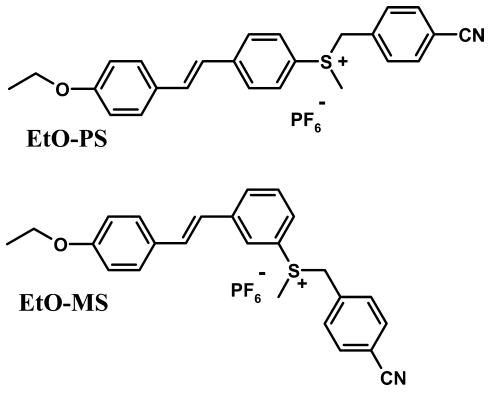

2. EXPERIMENTAL SECTION

2.1. Materials. All chemicals for synthesis were purchased from Sinopharm Chemical Reagent Co., Ltd., TCI, Alfa Aesar, or J&K Chemical, and they were used without further purification unless otherwise specified. Methylene chloride and acetonitrile were dried by calcium hydride refluxing for 24 h. All the solvents employed for photophysical measurements were Fluka spectroscopic grade. The cycloaliphatic diepoxide monomer, namely, 3,4-epoxycyclohexylmethyl-3,4-epoxycyclohexanecarboxylate, was supplied by Aldrich.

2.2. General Techniques. ^{1}H NMR was performed on Bruker-400 M to confirm the structures, and tetramethylsilane (TMS) was used as internal standard. High resolution MS was measured on an Agilent Technologies 6510 (Q-TOF) spectrometer using a dual ESI source.

The absorption measurements were carried out with Perkin-Elmer Lambda 2 or Shimadzu 2500 double beam UV−vis spectrophotometers. Steady-state fluorescence and phosphorescence spectra were collected from a FluoroMax-4 spectrofluorometer. Emission spectra are spectrally corrected, and fluorescence quantum yields included the correction due to solvent refractive index and were determined relative to quinine bisulfate in 0.05 M sulfuric acid (Φ = 0.52).[32]

Fluorescence lifetimes were obtained using a nano-LED emitting at 344 nm as an excitation source, with a nano-LED controller module, Fluorohub from IBH, operating at 1 MHz. The detection was based on a R928P type photomultiplier from Hamamatsu with high sensitivity photon-counting mode. The decays were fitted with the iterative reconvolution method on the basis of the Marquardt−Levenberg algorithm.[33] Such a reconvolution technique[34] allows an overall-time resolution down to 0.2 ns. The quality of the exponential fits was checked using the reduced χ^2 ($\leq$1.2).

The steady-state anisotropy measurements were performed in a glassy matrix of ethanol at 77 K. The samples are placed in a 5-mm diameter quartz tube inside a Dewar filled with liquid nitrogen. Two Glan-Thompson polarizers are placed in the excitation and emission beams. The anisotropy r is determined as follows: $r = (I_{VV} - gI_{VH})/(I_{VV} + 2gI_{VH})$, where $g = (I_{HV})/(I_{HH})$, I is the fluorescence intensity, the subscripts denote the orientation (horizontal H or vertical V) of the excitation and emission polarizers, respectively, and g is an instrumental correction factor. The proper calibration of the setup was checked using a standard method[35] with rhodamine 101 in glycerol.

The cyclic voltammetry experiments[36] (using a computer-controlled Radiometer Voltalab 6 potentiostat with a three-electrode single-compartment cell; the working electrode was a platinum disk; a saturated calomel electrode (SCE) used as a reference was placed in a separate compartment) were performed at 300 K, in N_2-degassed acetonitrile with a constant concentration (0.1 M) of $(n\text{-Bu})_4BF_4$. Ferrocene was used as an internal reference.

The photoacid generation quantum yields were measured using rhodamine B base as acid indicator.[37] A low pressure Hg lamp equipped with band-pass filters was used as light source and the photon doses at 313 and 351 nm were determined by ferrioxalate actinometry.[38] Acetonitrile solutions of **EtO-PS** were irradiated at 351 nm, and solutions of **EtO-MS** were irradiated at 313 nm. The absorbance at excitation wavelength was greater than 2.5 to assume a total absorption of the incident photons. In parallel with the determination of the photoacid generation quantum yields, the photolysis quantum yields were evaluated by plotting the decrease of the absorbance at the maximum absorption wavelength (λ_{abs}) in function of the time of irradiation. The photolysis quantum yield was then derived from the slope at t = 0, corrected by the photon flux and the extinction coefficient at λ_{abs}.[38]

The concentration of generated acid upon two-photon excitation was also titrated using rhodamine B base as an acid indicator. All the experiments were carefully carried out in the dark to avoid photogeneration of acid due to parasite light. Typically, a solution of acetonitrile with the PAG (5×10^{-4} M) was two-photon irradiated for 15 min. An excess of rhodamine B (2×10^{-5} M) was then added to the sample. The concentration of the photogenerated acid was spectrophotometrically evaluated from the absorbance of protonated rhodamine B base. Each measurement was reproduced three times, which leads to an average value of H^+ concentration.

The two-photon absorption cross sections were measured at 730 nm by using open-aperture Z-scan method[39,40] with a femtosecond mode-locked Ti:sapphire laser (Spectra-Physics, Mai Tai; pulse duration $\sim$ 100 fs; repetition rate, 80 MHz; wavelength range, 690−1020 nm). After passing through a beam expander (×4), the laser beam is focused using an f = 10 cm lens and passed through a quartz cell (1 mm optical path length). The position of the sample cell is varied along the laser-beam direction (z-axis) using a Z-step motorized stage controlled by a computer. At constant incident excitation, the local power density within the sample is changed, and the corresponding transmitted laser beam, $T(z)$, recorded with a silicon photodetector (Ophir PD300), is monitored in connection with the z-position of the cell. The on-axis peak intensity of the incident pulses at the focal point, I_0, ranged from 35 to 50 GW cm^{-2}. If we assume that the linear absorption of the sample is negligible at working wavelength and that the laser exhibits a Gaussian beam profile in space and time, the nonlinear absorption coefficient β can be calculated from the curve fitting to the experimental transmittance with the following equation:

dx.doi.org/10.1021/cm2030075 | Chem. Mater. 2012, 24, 237−244

Scheme 2. (a) Ph_3MePBr, NaH, DMSO, 85°C (b) $Pd(OAc)_2$, $N(CH_2CH_2OH)_3$, 120°C (c) 4-cyanobenzyl bromide, CF_3SO_3Ag, CH_2Cl_2, −20°C (d) KPF_6 (3 equiv), water/acetone

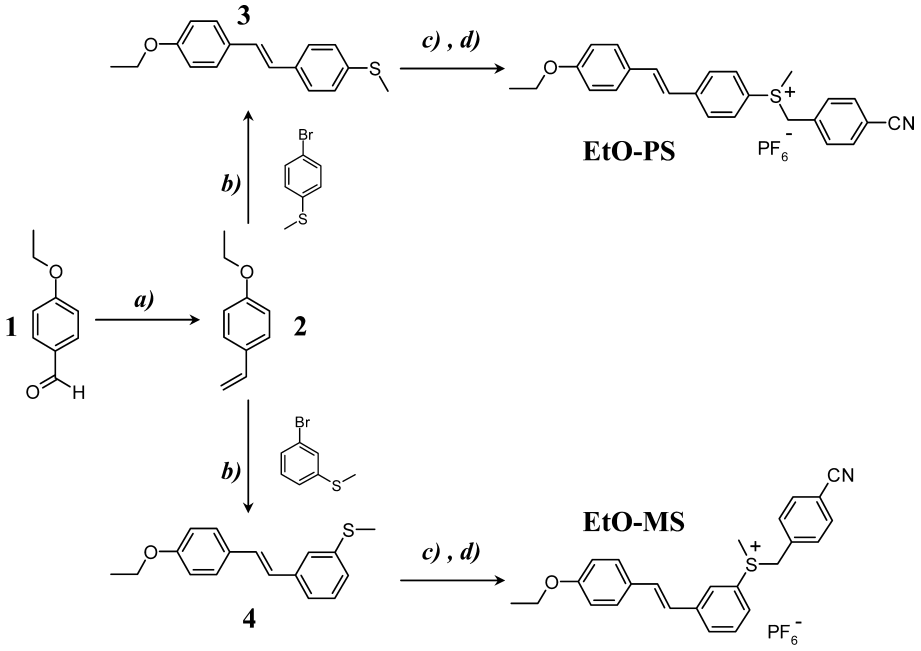

$$T(z) = 1 - \frac{\beta l I_0}{2\sqrt{2}\left(1 + \left(\frac{z}{z_0}\right)^2\right)} \quad (1)$$

where z_0 is the coordinate along the propagation direction of the focal point of the beam and l is the optical path length. The 2PA cross-section, δ, (in units of 1 GM:10^{-50} cm^4 s $photon^{-1}$ $molecule^{-1}$) is then determined by using the relationship:

$$\beta = \frac{\delta N_A d}{h\nu} 10^{-3} \quad (2)$$

where h is the Planck constant, ν the frequency of the incident laser beam, N_A the Avogadro constant, and d is the concentration of the chromophore (mol L^{-1}). The rhodamine 6G in methanol[41] (16.2 ± 2.4 GM at 806 nm) was used for the calibration of our measurement technique (see Figure S2 in the Supporting Information) . The uncertainty in δ is on the order of 20%.

The photopolymerization was monitored *in situ* by Fourier transform real-time infrared spectroscopy (FT-RTIR) with an AVATAR 360 FTIR spectrometer from Nicolet. A drop of the photocurable formulation is deposited on a KBr pellet then spread out with a calibrated bar. The aerated film, which exhibits an average thickness of 40 μm, is irradiated at 365 nm using a Xe−Hg lamp (Hamamatsu, L8252, 150 W) equipped with a band-pass filter. The UV light irradiance was maintained to a value of 3.5 mW cm^{-2}. The conversion rates are derived from the changes in the infrared absorption bands of the monomer. The regions of interest correspond to the decrease in the epoxide absorption bands in the 800−900 cm^{-1} region, which corresponds to the C−H bond stretching vibration of epoxide and to the increase of the peaks at 1050−1150 cm^{-1} assigned to the absorption of the (C−O−C) groups in the poly(ether), which is produced upon photopolymerization.[42,43]

The 3D lithographic microfabrication was performed using a Zeiss Axio Observer D1 inverted microscope equipped with a frequency doubled Nd:YAG microlaser Nanolase from JDS Uniphase (λ_{exc} = 532 nm; pulse duration, 0.61 ns; maximum pulse energy, 6 μJ; repetition, 11.8 kHz). The two-photon excitable resin was sandwiched between two coverslips, and then, mounted on a computer-controlled 3D piezoelectric stage, allowing the translation relative to the laser focal point. The incident beam was focused through a 0.65 NA objective (40×) that leads to 400 nm radial spot size (1/e Gaussian). The average laser power was 220 μW. This entire lithography setup was purchased from Teem Photonics.

2.3. Synthesis. The synthetic route for the synthesis of both chromophores is depicted in Scheme 2. Previously reported procedures were used to prepare 4-ethoxybenzaldehyde[44] **1** and 3-bromothioanisole.[45]

4-Ethoxystyrene ***2.*** NaH (60%, 2.8 g, 70 mmol) was suspended in a solution of methyltriphenylphosphonium bromide (21 g, 60 mmol) in DMSO (80 mL). This reaction mixture was stirred under N_2 at 85 °C for 60 min to form orange phosphonium ylide. The obtained solution was then allowed to reach room temperature (RT). 4-Ethoxybenzaldehyde (9 g, 60 mmol) was added dropwise. This reaction mixture was stirred at RT for 2 h under Ar, poured into cold water, and extracted three times with Et_2O. The combined organic layer was extracted with brine, dried over $MgSO_4$, and evaporated under reduced pressure. Purification by flash column chromatography (CH_2Cl_2/petroleum ether 1:10) afforded pure 4-ethoxystyrene **2** (7 g, 80%) as a colorless liquid. The spectroscopic data obtained were in agreement with those of a commercial sample.

4-Ethoxy-4′-methylthiostilbene 3 and 4-Ethoxy-3′-methylthiostilbene 4. A suspension of bromothioanisole (1 equiv), 4-ethoxystyrene (1 equiv), and $Pd(OAc)_2$ (0.01 equiv) in triethanolamine (2 mL per 1 mmol of bromoanisole) was heated under stirring at 100 °C for 10 h under Ar. The reaction mixture was then poured into water. The precipitate obtained was filtered and dissolved in CH_2Cl_2. Filtration through a short pad of silica gel, followed by a recrystallization from ethanol/CH_2Cl_2, afforded the desired stilbenes **3** and **4**.

Compound ***3.*** Starting from 4-ethoxystyrene (148 mg, 1 mmol) and 4-bromothioanisole (203 mg, 1 mmol), **3** was obtained (170 mg, 63%) as a white powder. ^{1}H NMR (400 MHz, $CDCl_3$, δ_{ppm}): 7.42 (d, J = 8.8 Hz, 2H, H_2); 7.40 (d, J = 8.4 Hz, 2H, $H_{2'}$); 7.23 (d, J = 8.4 Hz, 2H, $H_{3'}$); 7.02 (d, J = 16.3 Hz, 1H, H_{vinyl}); 6.91 (d, J = 16.3 Hz, 1H, $H_{vinyl(ethoxyphenyl)}$); 6.88 (d, J = 8.8 Hz, 2H, H_3); 4.05 (q, J = 7.0 Hz, 2H, CH_2); 2.50 (s, 3H, S−CH_3); 1.42 (t, J = 7.0 Hz, 3H, CH_3).

Compound ***4.*** Starting from 4-ethoxystyrene (148 mg, 1 mmol) and 3-bromothioanisole (203 mg, 1 mmol), **4** was obtained (165.7 mg, 61.5%) as a white powder. ^{1}H NMR (400 MHz, $CDCl_3$, δ_{ppm}): 7.53 (d, J = 8.8 Hz, 2H, H_2); 7.44 (t, J = 1.5 Hz, 1H, $H_{2'}$); 7.34 (dt, J = 7.7 Hz, J = 1.5 Hz, 1H, $H_{6'}$); 7.29 (t, J = 7.7 Hz, 1H, $H_{5'}$); 7.23 (d, J = 16.5

dx.doi.org/10.1021/cm2030075 | *Chem. Mater.* 2012, 24, 237−244

Hz, 1H, H_{vinyl}); 7.12 (dt, J = 7.7 Hz, J = 1.5 Hz, 1H, $H_{4'}$); 7.06 (d, J = 16.5 Hz, 1H, $H_{vinyl(ethoxyphenyl)}$); 6.93 (q, J = 8.8 Hz, 2H, H_3); 4.04 (q, J = 6.9 Hz, 2H, CH_2); 2.51 (s, 3H, S−CH_3); 1.33 (t, J = 6.9 Hz, 3H, CH_3).

4-Ethoxy-4′-methyl(*p*-cyanobenzyl)sulfonium Stilbene Hexafluorophosphate (EtO-PS) and 4-Ethoxy-3′-methyl(*p*-cyanobenzyl)sulfonium Stilbene Hexafluorophosphate (EtO-MS). According to the literature,[31] 4-ethoxy methylstilbenes **3** and **4** were converted into their trifluoromethanesulfonate salts. Then, anion-exchange of $CF_3SO_3^-$ by PF_6^- was performed using the Zhou et al. method,[14] leading to the final products **EtO-PS** and **EtO-MS**. Both PAGs are stable in the dark and can be stored several months at room temperature without any decomposition. They show a good solubility in organic solvents, such as acetone, tetrahydrofuran, acetonitrile, methylene chloride, and chloroform.

EtO-PS. Starting from **3** (270 mg, 1 mmol), **EtO-PS** (398 mg, 75%) was obtained as a pale powder. ^{1}H NMR (400 MHz, CD_3CN, δ_{ppm}): 7.76 (d, J = 8.6 Hz, 2H, $H_{3'}$); 7.71 (d, J = 8.2 Hz, 2H, $H_{2\ benzonitrile}$); 7.65 (d, J = 8.6 Hz, 2H, $H_{2'}$); 7.56 (d, J = 8.7 Hz, 2H, H_2); 7.39 (d, J = 16.4 Hz, 1H, H_{vinyl}); 7.36 (d, J = 8.2 Hz, 2H, $H_{3benzonitrile}$); 7.11 (d, J = 16.4 Hz, 1H, $H_{vinyl(ethoxyphenyl)}$); 6.95 (d, J = 8.7 Hz, 2H, H_3); 4.90 (d, J = 12.8 Hz 1H, S−CH_2); 4.72 (d, J = 12.8 Hz, 1H, S-CH_2); 4.08 (q, J = 7.0 Hz, 2H, O−CH_2); 3.19 (s, 3H, S−CH_3); 1.37 (t, J = 7.0 Hz, 3H, C−CH_3). ^{13}C NMR (100.6 MHz, CD_3CN, δ_{ppm}): 15.03; 25.91; 50.98; 64.44; 114.38; 115.71; 118.9; 119.47; 124.47; 128.89; 129.54; 129.77; 132.29; 132.44; 133.81; 133.98; 134.12; 145.55; 160.63. HRMS (ESI-Q-TOF) m/z calcd. for $[C_{25}H_{24}NOS]^{*\,+}$: 386.1573. Found: 386.1568.

EtO-MS. Starting from **4** (1 g, 3.7 mmol), **EtO-Ms** (1.321 g, 67%) was obtained as a yellow powder. ^{1}H NMR (400 MHz, CD_3CN, δ_{ppm}): 7.87 (d, J = 7.9 Hz, 1H, $H_{4'}$); 7.79 (t, J = 1.5 Hz, 1H, $H_{2'}$); 7.71 (d, J = 8.3 Hz, 2H, $H_{2benzonitrile}$); 7.56 (t, J = 7.9 Hz, 1H, $H_{5'}$); 7.53 (d, J = 8.7 Hz, 2H, H_2); 7.50 (d, J = 7.9 Hz, 1H, $H_{6'}$); 7.35 (d, J = 8.3 Hz, 2H, $H_{3benzonitrile}$); 7.26 (d, J = 16.5 Hz, 1H, H_{vinyl}); 7.06 (d, J = 16.5 Hz, 1H, $H_{vinyl(methoxyphenyl)}$); 6.95 (d, J = 8.7 Hz, 2H, H_3); 4.91 (d, J = 12.9 Hz, 1H, S-CH_2); 4.73 (d, J = 12.9 Hz, 1H, S−CH_2); 4.08 (q, J = 7.0 Hz, 2H, O−CH_2); 3.21 (s, 3H, S−CH_3); 1.37 (t, J = 7.0 Hz, 3H, C−CH_3). ^{13}C NMR (100.6 MHz, CD_3CN, δ_{ppm}): 15.04; 25.52; 50.70; 64.41; 114.42; 115.70; 118.88; 123.42; 124.15; 128.49; 129.27; 129.75; 129.87; 131.98; 132.47; 132.72; 133.21; 133.71; 133.97; 141.91; 160.41. HRMS (ESI-Q-TOF) m/z calcd. for $[C_{25}H_{24}NOS]^{*\,+}$: 386.1573. Found: 386.1568.

3. RESULTS AND DISCUSSION

Photophysical Properties of the Photoacid Generators. Figure 1 shows the absorption spectra of the PAGs in acetonitrile. The steady-state excitation anisotropies recorded in the glassy matrix of ethanol are also superimposed. All spectroscopic data are listed in Table 1. It is noteworthy that the absorption spectra of the chromophores are hardly sensitive to solvent polarity. Both spectra exhibit two well-separated bands. In the high energy side of the spectra, a distinctive band located at 230 nm is observed and exhibits a value of anisotropy close to 0.2 for each chromophore. This band mainly corresponds to the ^1L_a transition centered on alkoxyphenyl moiety.[46] Whereas the maximum wavelength of this band is insensitive to the position of the sulfonium substituent, its intensity clearly decreases by a factor 1.35 upon going from a meta to para compound. Reciprocally, the longest-wavelength absorption band located in the 275−415 nm range increases by a factor 1.5 and undergoes a remarkable redshift by 23 nm. These effects should be ascribed to a better π orbital overlap between the donor (i.e., alkoxyphenyl) and acceptor (i.e., phenylsulfonium) groups, which is promoted by a more planar conformation in the case of **EtO-PS**. Moreover, the anisotropy recorded within this spectral region exhibits a constant value of ca. 0.36 ± 0.02 and 0.32 ± 0.03 for para and meta derivatives, respectively. These constant anisotropies confirm that this absorption band is mainly dominated by a single transition, probably with $\pi-\pi^*$ character, and whose absorption transition moment is collinear with that of the emission one. Interestingly, the anisotropy decreases at the red edge of the absorption spectrum, which indicates the presence of another transition with a distinct electronic symmetry with respect to that of the $\pi-\pi^*$ one. The occurrence of this weakly allowed transition is also corroborated by the additional weak tail observed in the low energy side of the absorption spectrum of **EtO-MS**. In **EtO-PS**, the corresponding band is likely hidden by the $\pi-\pi^*$ transition, as revealed by the position of the anisotropy drop. Such a transition should be assigned to the $\pi-\sigma^*$ transition with a σ^* LUMO located on the sulfur−carbon (S−C) bond. As previously demonstrated by Saeva et al.,[47,48] efficient photoinduced cleavage of the C−S bond of sulfonium salts occurs when the lowest excited state is the $\pi-\sigma^*$ one. In this case, the main photocleavage properties are dependent on the energy gap between the σ^* LUMO and the next higher lying π^* MO. On the other hand, a crossover between the σ^* and π^* states induces a drastic decrease of the photodissociation ability of the sulfonium salt. According to the anisotropy signal, the $\pi-\sigma^*$ transition is lying at lower energy than the $\pi-\pi^*$ transition in both the **EtO-MS** and **EtO-PS** compounds, which excludes the presence of such a crossover. However, it is clear that the energy gap between these two electronic levels is decreasing upon going from the meta to the para derivative. Such a spectroscopic effect will have strong consequences on the photolysis properties of the PAGs, as described hereafter.

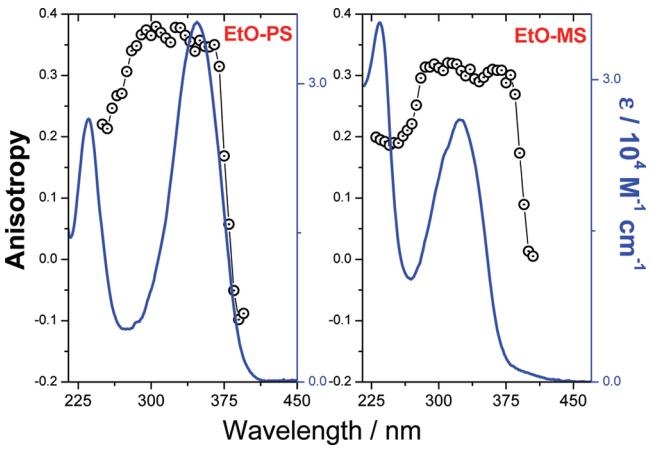

Figure 1. Absorption spectra of **EtO-PS** and **EtO-MS** in acetonitrile (full lines). Fluorescence excitation anisotropy (circles) in glassy matrix of EtOH at 77 K (**EtO-PS**: λ_{em} = 440 nm, **EtO-MS**: λ_{em} = 450 nm).

Both compounds exhibit very low fluorescence quantum yields ($\Phi_{fluo} < 10^{-2}$) and have short fluorescence lifetimes below 0.2 ns, which suggests that the lowest singlet excited states (S_1) mainly relax through nonradiative deactivation pathways, such as the S−C bond cleavage. As depicted in Figure 2, the absorption spectra of the chromophores undergo strong changes upon irradiation at 350 nm. Whereas the high energy band centered at 230 nm is slightly increasing during irradiation, the longest wavelength absorption band collapses dramatically in connection with the growth of new bands located in the 250−310 nm range. Moreover, an isosbestic point is observed at 284 nm for **EtO-MS** and at 307 nm for **EtO-PS**, which indicates an equilibrium reaction at ground state. It is to be noted that these nondegassed solutions exhibit

dx.doi.org/10.1021/cm2030075 | *Chem. Mater.* 2012, 24, 237−244

Table 1. Summary of Optical Data and Parameters for EtO-PS and EtO-MS

	λ_{abs} (nm)	ε^{MAX} (M^{-1} cm^{-1})[a]	λ_{fluo} (nm)	Φ_{fluo}[b]	τ_{fluo} (ns)	E_{00} (eV)	ΔG_{eT} (eV)[c]	Φ_{acid}[a]	λ^{2PA}(nm)	δ (GM)[b]
EtO-MS	324	26 000	382	0.004	<0.2	3.50	−1.23	0.24	710	68
EtO-PS	347	36 100	388	0.009	<0.2	3.24	−0.97	0.10	760	73

[a]Error is about 10%. [b]Error is about 20%. [c]Free energy calculated from eq 3. [b]The uncertainty in δ is of the order of 20%

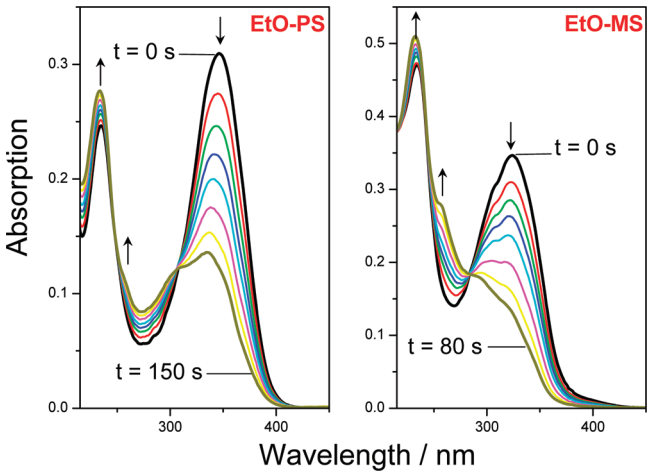

Figure 2. Evolution of the absorption spectra of the PAGs upon irradiation at 350 nm (solvent: acetonitrile).

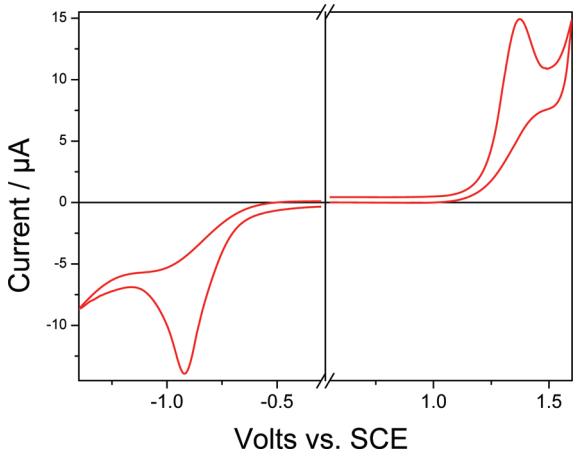

Figure 3. Cyclic voltamogramm of **EtO-MS** in acetonitrile + $(n\text{Bu})_4NPF_6$ (0.1 M) on platinum electrode at 100 mV s^{-1} ([**EtO-PS**]: 3 × 10^{-3} M).

rates of photolysis equivalent to those obtained for nitrogen-degassed solutions. This is a clear indication that the reaction is insensitive to the presence of oxygen and should thus occur at the singlet excited level rather than the triplet one. A bond cleavage mechanism promoted by an intramolecular photoinduced electron transfer (PET) at S_1 state is also supported by the estimation of the free energy (ΔG_{eT}) associated to this process. We calculated ΔG_{eT} using Rehm−Weller eq 3:[49]

$$\Delta G_{eT} = E_{ox} - E_{red} - E_{00} - C \quad (3)$$

In this formalism, E_{ox} and E_{red} correspond to the oxidation and reduction potentials of the donor and acceptor, respectively. E_{00} is the energy of singlet excited state, which is calculated by Berlman's method.[50] C is the Coulombic energy term characterizing the interaction of the radical ion pairs. In acetonitrile, this term usually makes a small contribution to the overall energy change for PET and was neglected in the calculation, as previously assumed for other sulfonium-based derivatives.[14] The values of E_{ox} and E_{red} are determined from cyclic voltammetry. Figure 3 displays the cyclic voltamogramm of **EtO-MS** in acetonitrile. It is to be noted that **EtO-PS** has a similar electrochemical fingerprint. Each compound exhibits an irreversible electrochemical reduction wave with a peak at −0.89 V and −0.92 V vs SCE for **EtO-MS** and **EtO-PS**, respectively. These cathodic potentials should be assigned to the one-electron reduction of the sulfonium group, in good accordance with those measured for similar methyl(*p*-cyanobenzyl)sulfonium cations.[31] Such an electrochemical reduction is generally irreversible because of the carbon−sulfur σ-bond cleavage leading to the production of a sulfide and a carbon-centered radical. Interestingly, the change in reduction potentials within a series of compounds can be considered as a measure of the energy of the S−C bond σ^* orbital. In this regard, the similar E_{red} values in **EtO-MS** and **EtO-PS** indicate that the para to meta substitution hardly affects the relative position of the σ^*-LUMO. As a consequence, the decrease of the energy gap between the σ^* and π^* MOs mainly stems from the strong stabilization of the π^* level, as depicted in Scheme 3. At high potential, both chromophores show a similar

Scheme 3. Evolution of the Two Low-Lying Levels Disposition upon Going from EtO-PS to EtO-MS

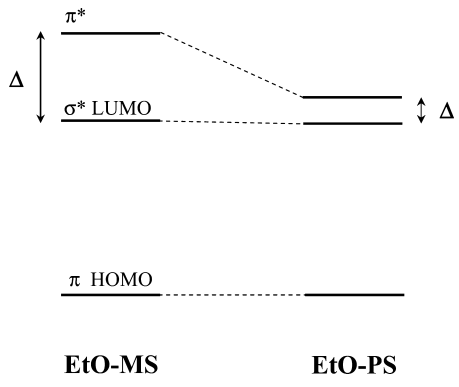

irreversible wave with a peak at 1.35 V vs SCE, which corresponds to the oxidation of the electron-rich part of the chromophores. Interestingly, this oxidation potential is lower than that of anisole (1.65 V vs SCE); therefore, the vinyl function should be involved in the stabilization of the generated dication. According to the redox potentials, ΔG_{eT} values have been estimated and are listed in Table 1. In both cases, the intramolecular electron transfer at the S_1 state is largely exergonic, while it is thermodynamically forbidden at the ground state ($\Delta G_{eT} > 0$). Moreover, this driving force is more exergonic by 0.26 eV for **EtO-MS** than for **EtO-PS**, which is due to a much lower singlet state energy. The photoacid generation quantum yields (Φ_{acid}) were evaluated using the method previously reported by Scaiano et al.[37] **EtO-MS** and **EtO-PS** were irradiated at 313 and 351 nm, respectively, which corresponds to the π−π^* excitation. The photodecomposition

dx.doi.org/10.1021/cm2030075 | *Chem. Mater.* 2012, 24, 237−244

conversion was recorded for values lower than 5%, so as to neglect the interferences from secondary photoproducts. As shown in Figure 4, the concentration of the photogenerated acid increases linearly with the absorbed photon dose. From the

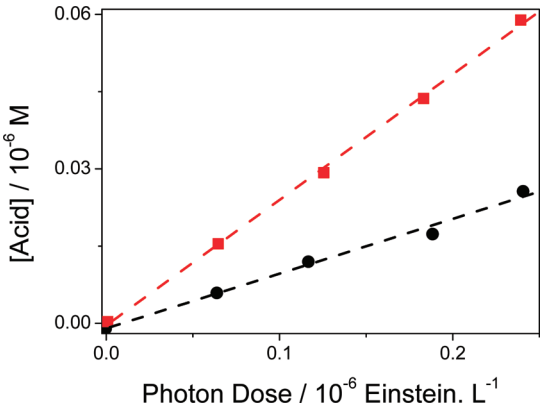

Figure 4. Concentration of photogenerated acid as function of the absorbed photon in acetonitrile (Circles: **EtO-PS**. Squares: **EtO-MS**).

linear relationships, it is clear that the slope related to the meta compound is higher than that for the para one. The quantum yields for acid generation (Φ_{acid}) are gathered in Table 1. We can then observe that **EtO-MS** exhibits a remarkable Φ_{acid} of ca. 0.24, which is more than twice higher ($\sim$ 2.4) than the value found for its para isomer. Interestingly, the photolysis quantum yield of the meta derivative (ca. 0.29) is also 2.6 times larger than that measured for **EtO-PS**. Such equivalent ratios first suggest that the chemical rearrangement consecutive to the primary photocleavage[31,51−53] process has similar kinetics for both PAGs and that the enhancement in acid generation is mainly ascribed to a more efficient S−C bond dissociation ability for **EtO-MS**. This photocleavage enhancement is a direct consequence of a better energy separation between the σ^* LUMO and its high lying π^* MO. Indeed, a weak gap (**Δ** in Scheme 3) promotes the electronic coupling between these two MOs, which should reduce the dissociative character of the LUMO.

Photoinitiated Cationic Polymerization. The more efficient acid generation observed for **EtO-MS**, as compared to **EtO-PS**, has a direct effect on the cationic photoionitiating properties of each photoacid generator. Figure 5 shows the FT-RTIR kinetic curves for difunctional epoxide formulations containing the PAGs, which are irradiated at 365 nm. The concentration of the PAGs was adjusted so that each sample exhibits a similar absorbance at the excitation wavelength. Whereas the conversion of epoxide hardly reached 25% after 120 s irradiation for the para compound, this conversion is multiplied by a factor of 2 for the **EtO-MS**. In the same manner, the initial rate of photopolymerization for **EtO-MS** is 1.7 higher than that measured for **EtO-PS**. Hence, the meta derivative clearly shows higher photoinitiating reactivity than the para isomer. It is noteworthy that, even in highly viscous monomer, we have no leveling effect and a good correlation is maintained between the acid generation quantum yield and the cationic photoinitiation reactivity.

Two-Photon Absorption Properties. The two-photon absorption (2PA) spectra of the PAGs have been measured in the 700−800 nm range using the open aperture Z-scan technique (see Figures S2 and S3 in the Supporting

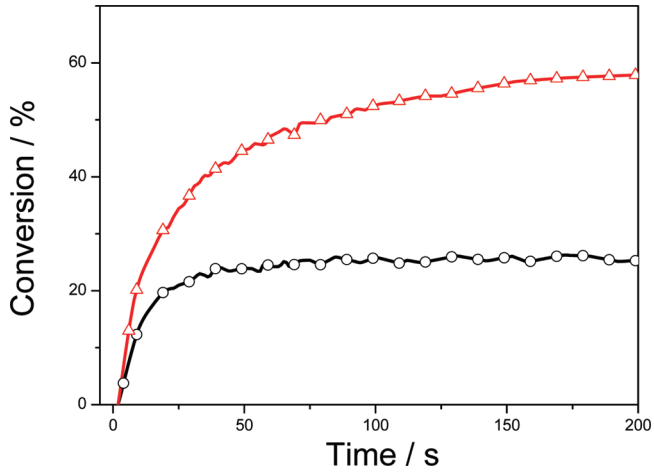

Figure 5. Conversion vs time curves for cationic photopolymerization of diepoxide monomer. λ_{exc}: 365 nm. Irradiance: 3.5 mW cm^{-2}. Photoinitiating systems: **EtO-PS**, 0.4 wt % (circles), **EtO-MS**, 1.6 wt % (triangles).

Information). Figure 6 shows the one- (full line) and two-photon (data points) absorption spectra of the compounds.

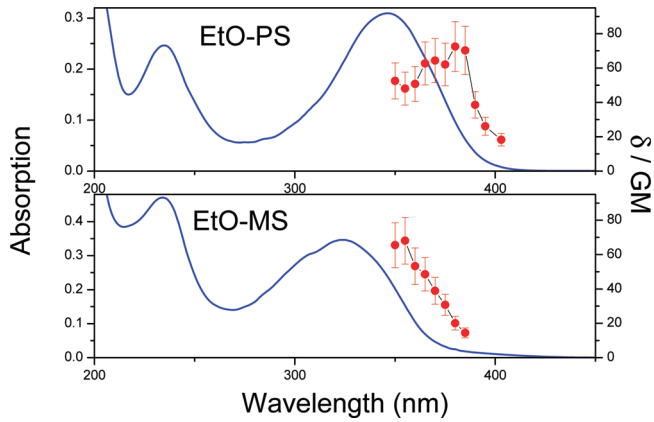

Figure 6. One- (full lines) and two- (data points) photon absorption spectra of photoacid generators (solvent: acetonitrile).

The 2PA spectra are plotted against half the excitation wavelength. The 2PA spectrum of the two photoacid generators consists of a low intensity band with a maximum located near 760 and 710 nm for **EtO-PS** and **EtO-MS**, respectively. This band does not coincide with the lowest one-photon absorption band and should be ascribed to the two-photon excitation of the weakly allowed S_0−S_1 transition (π−σ^* type), which is located in the low energy side of the one-photon absorption spectrum, as previously indicated. The 2PA cross sections at the maximum absorption are of the same order of magnitude with values close to 70 GM for both PAGs (see Table 1). Therefore, it is of interest to note that the para-to-meta substitution strategy does not exhibit detrimental effects toward the 2PA ability of these push−pull stilbenes but leads to a sizable increase of the acid generation.

To show that acid generation can be two-photon activated with **EtO-PS** and **EtO-MS**, we measured the acid yield in function of the excitation intensity at 730 nm. As shown in Figure 7, the concentration of the photogenerated acid, which was determined spectrophotometrically with rhodamine B, increases with the square of the excitation power. This

dx.doi.org/10.1021/cm2030075 | *Chem. Mater.* 2012, 24, 237−244

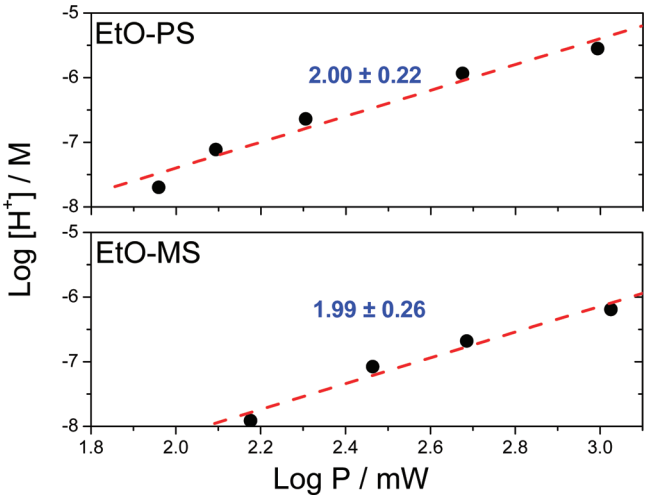

Figure 7. Plots of log[H^+] vs log[excitation power] at 730 nm.

quadratic relationship is consistent with a photochemical reaction, which is two-photon activated.

Two-Photon Microfabrication. To demonstrate the potential applications of our photoacid generators in two-photon photopolymerization, 2D microstructures were produced using the same difunctional epoxide formulation as that previously employed for one-photon photopolymerization. For this purpose, the resin was excited at 532 nm with a nanosecond pulse microlaser. At this time-scale excitation, it should be pointed out that a stepwise two-photon absorption process is excluded because of the very short lifetimes of singlet excited states (τ_{fluo} < 0.2 ns). Moreover, it has been previously demonstrated for ionic push−pull systems[54] or for porphyrin derivatives[55−57] that a strong enhancement of 2PA cross-section is observed nearby the one-photon absorption region. In line with this strategy, we also assume a one-photon resonance enhancement for our sulfonium photoacid generators. Figure 8 shows examples of optical transmission microscopy images of 2D-microstructures written within the resin containing **EtO-MS** and using a 40 × 0.65 NA objective. The patterns were fabricated at low incident power of 220 μW. These 2D-microstructures first indicate that the meta derivative can be two-photon activated near its one-photon-allowed absorption region and also illustrate the potential interest of **EtO-MS** in microfabrication domain.

CONCLUSION

Two positional isomers of a 4-alkoxystilbene substituted with a methyl (*p*-cyanobenzyl) sulfonium group have been designed and synthesized. The photophysical features of these new photoacid generators have been described and compared with each other, so as to highlight some relevant structure−properties relationships in connection with the substitution strategy. Both systems undergo an S−C bond cleavage at singlet excited state promoted by an intramolecular PET process. However, upon going from **EtO-PS** to **EtO-MS**, a clear enhancement of the photolysis efficiency is observed as a result of the increase of the energy gap between the dissociative σ^* LUMO and the high lying π^* MO. The quantum yield of acid generation is consequently multiplied by a factor of 2.4, which is nicely corroborated in cationic photopolymerization by a strong increase in the photoinitiating reactivity. Interestingly, such a substitution approach hardly affects the two-photon absorption ability of the donor−acceptor stilbene system, which exhibits δ^{MAX} close to 70 GM in the 700−800 nm range. We finally show that **EtO-MS** is of potential interest for two-photon initiating polymerization when excited near its one-photon absorption band.

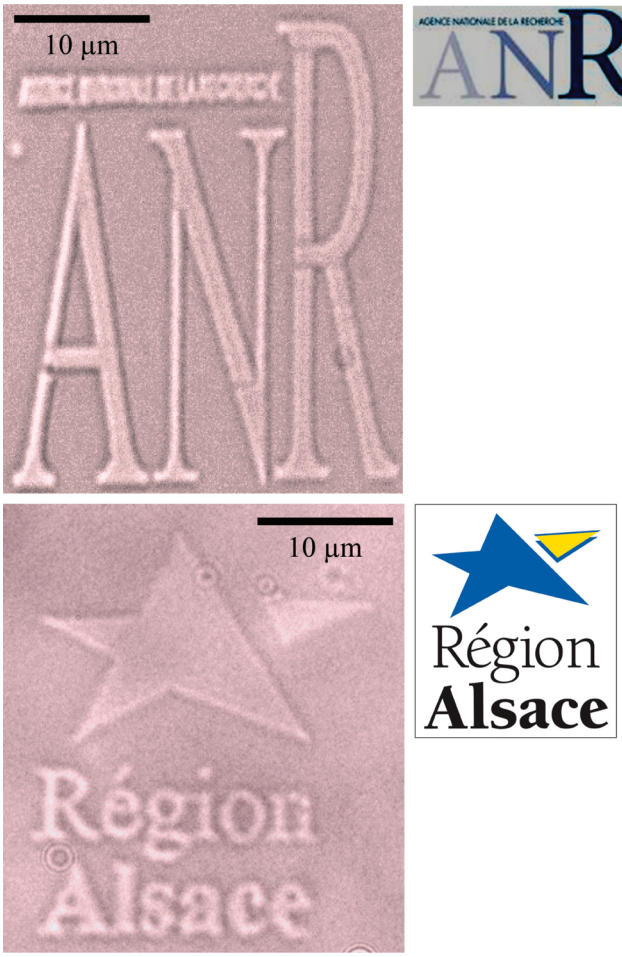

Figure 8. Microstructures fabricated by two-photon induced polymerization upon excitation at 532 nm. (Diepoxide resin with **EtO-MS**, 1.6 wt %. Power: 220 μW.)

ASSOCIATED CONTENT

Supporting Information

Additional graphs and figures. This material is available free of charge via the Internet at http://pubs.acs.org.

AUTHOR INFORMATION

Corresponding Authors

*E-mail: jean-pierre.malval@uha.fr.
*E-mail: mingjin@tongji.edu.cn.

ACKNOWLEDGMENTS

We thank the National Natural Science Foundation of China (No. 20902069) and the program for Young Excellent Talents in Tongji University (No. 2008KJ002) for financial support. Support from the Agence Nationale de la Recherche "Projet Blanc: *2PAGmicrofab* (ANR-BLAN-0815-03) " and "Retour Post-Doc: *Nanoquenching* (10DOC-009 01) " are also gratefully acknowledged.

REFERENCES

(1) Reichmanis, E.; Thompson Larry, F. In *Polymers in Microlithography*; American Chemical Society: Washington DC, 1989; Vol. *412*, pp 1−24.
(2) Reichmanis, E.; Houlihan, F. M.; Nalamasu, O.; Neenan, T. X. In *Polymers for Microelectronics*; American Chemical Society: Washington DC, 1993; Vol. *537*, pp 2−24.
(3) Shirai, M.; Tsunooka, M. *Prog. Polym. Sci.* **1996**, *21*, 1−45.
(4) Lee, K.-S.; Kim, R. H.; Yang, D.-Y.; Park, S. H. *Prog. Polym. Sci.* **2008**, *33*, 631−681.
(5) Lee, K.-S.; Yang, D.-Y.; Park, S. H.; Kim, R. H. *Polym. Adv. Technol.* **2006**, *17*, 72−82.
(6) Chochos, C. L.; Ismailova, E.; Brochon, C.; Leclerc, N.; Tiron, R.; Sourd, C.; Bandelier, P.; Foucher, J.; Ridaoui, H.; Dirani, A.; Soppera, O.; Perret, D.; Brault, C.; Serra, C. A.; Hadziioannou, G. *Adv. Mater.* **2009**, *21*, 1121−1125.
(7) Sun, H.-B.; Kawata, S. *Two-Photon Photopolymerization and 3D Lithographic Microfabrication*; Springer-Verlag: Berlin, 2004; Vol. *170*.
(8) Malval, J.-P.; Morlet-Savary, F.; Allonas, X.; Fouassier, J.-P.; Suzuki, S.; Takahara, S.; Yamaoka, T. *Chem. Phys. Lett.* **2007**, *443*, 323−327.
(9) Malval, J.-P.; Suzuki, S.; Morlet-Savary, F.; Allonas, X.; Fouassier, J.-P.; Takahara, S.; Yamaoka, T. *J. Phys. Chem. A* **2008**, *112*, 3879−3885.
(10) Shirai, M.; Okamura, H. *Prog. Org. Coat.* **2009**, *64*, 175−181.
(11) Ortica, F.; Coenjarts, C.; Scaiano, J. C.; Liu, H.; Pohlers, G.; Cameron, J. F. *Chem. Mater.* **2001**, *13*, 2297−2304.
(12) Arnold, P. A.; Fratesi, L. E.; Bejan, E.; Cameron, J.; Pohlers, G.; Liu, H.; Scaiano, J. C. *Photochem. Photobiol. Sci.* **2004**, *3*, 864−869.
(13) Ortica, F.; Scaiano, J. C.; Pohlers, G.; Cameron, J. F.; Zampini, A. *Chem. Mater.* **2000**, *12*, 414−420.
(14) Zhou, W.; Kuebler, S. M.; Carrig, D.; Perry, J. W.; Marder, S. R. *J. Am. Chem. Soc.* **2002**, *124*, 1897−1901.
(15) Farrer, R. A.; LaFratta, C. N.; Li, L.; Praino, J.; Naughton, M. J.; Saleh, B. E. A.; Teich, M. C.; Fourkas, J. T. *J. Am. Chem. Soc.* **2006**, *128*, 1796−1797.
(16) Cumpston, B. H.; Ananthavel, S. P.; Barlow, S.; Dyer, D. L.; Ehrlich, J. E.; Erskine, L. L.; Heika, A. A.; Kuebler, S. M.; Lee, I.-Y. S.; McCord-Maughon, D.; Qin, J.; Röckel, H.; Rumi, M.; Wu, X.-L.; Marder, S. R.; Perry, J. W. *Nature* **1999**, *398*, 51−54.
(17) Kawata, S.; Sun, H.-B. *Appl. Surf. Sci.* **2003**, *208*−*209*, 153−158.
(18) He, G. S.; Tan, L.-S.; Zheng, Q.; Prasad, P. N. *Chem. Rev.* **2008**, *108*, 1245−1330.
(19) Malval, J.-P.; Morlet-Savary, F.; Chaumeil, H. l. n.; Balan, L.; Versace, D.-L.; Jin, M.; Defoin, A. *J. Phys. Chem. C* **2009**, *113*, 20812−20821.
(20) Narewska, J.; Strzelczyk, R.; Podsiadly, R. *J. Photochem. Photobiol., A* **2010**, *212*, 68−74.
(21) Gómez, M. L.; Previtali, C. M.; Montejano, H. A.; Bertolotti, S. G. *J. Photochem. Photobiol., A* **2007**, *188*, 83−89.
(22) Cho, J.-D.; Hong, J.-W. *Eur. Polym. J.* **2005**, *41*, 367−374.
(23) Li, C.; Luo, L.; Wang, S.; Huang, W.; Gong, Q.; Yang, Y.; Feng, S. *Chem. Phys. Lett.* **2001**, *340*, 444−448.
(24) Billone, P. S.; Park, J. M.; Blackwell, J. M.; Bristol, R.; Scaiano, J. C. *Chem. Mater.* **2009**, *22*, 15−17.
(25) Steidl, L.; Jhaveri, S. J.; Ayothi, R.; Sha, J.; McMullen, J. D.; Ng, S. Y. C.; Zipfel, W. R.; Zentel, R.; Ober, C. K. *J. Mater. Chem.* **2009**, *19*, 505−513.
(26) Kuebler, S. M.; Braun, K. L.; Zhou, W.; Cammack, J. K.; Yu, T.; Ober, C. K.; Marder, S. R.; Perry, J. W. *J. Photochem. Photobiol., A* **2003**, *158*, 163−170.
(27) Zhou, W.; Kuebler, S. M.; Braun, K. L.; Yu, T.; Cammack, J. K.; Ober, C. K.; Perry, J. W.; Marder, S. R. *Science* **2002**, *296*, 1106−1109.
(28) Yu, T.; Ober, C. K.; Kuebler, S. M.; Zhou, W.; Marder, S. R.; Perry, J. W. *Adv. Mater.* **2003**, *15*, 517−521.
(29) Yanez, C. O.; Andrade, C. D.; Belfield, K. D. *Chem. Commun.* **2009**, 827−829.
(30) Beak, P.; Sullivan, T. A. *J. Am. Chem. Soc.* **1982**, *104*, 4450−4457.
(31) Saeva, F. D.; Morgan, B. P. *J. Am. Chem. Soc.* **1984**, *106*, 4121−4125.
(32) Meech, R.; Phillips, D. *J. Photochem.* **1983**, *23*, 193−217.
(33) Connor, D. V.; Phillips, D. *Time Correlated Single Photon Counting*; Academic Press: London, 1984.
(34) Ven, M. V. D.; Ameloot, M.; Valeur, B.; Boens, N. *J. Fluoresc.* **2005**, *15*, 377−413.
(35) Prazeres, T. J. V.; Fedorov, A.; Barbosa, S. P.; Martinho, J. M. G.; Berberan-Santos, M. r. N. *J. Phys. Chem. A* **2008**, *112*, 5034−5039.
(36) Malval, J.-P.; Chaimbault, C.; Fischer, B.; Morand, J.-P.; Lapouyade, R. *Res. Chem. Intermed.* **2001**, *27*, 21−34.
(37) Pohlers, G.; Scaiano, J. C.; Sinta, R. *Chem. Mater.* **1997**, *9*, 3222−3230.
(38) Montalti, M.; Credi, A.; Prodi, L.; Gandolfi, M. T. *Handbook of Photochemistry*, 3rd ed.; CRC Press: Boca Raton, FL, 2006.
(39) Sheik-Bahae, M.; Said, A. A.; Wei, T. H.; Hagan, D. J.; Stryland, E. W. V. *IEEE J. Quantum Electron.* **1990**, *26*, 760.
(40) Sheik-Bahae, M.; Said, A. A.; Stryland, E. W. V. *Opt. Lett.* **1989**, *14*, 955−957.
(41) Sengupta, P.; Balaji, J.; Banerjee, S.; Philip, R.; Kumar, G. R.; Maiti, S. *J. Chem. Phys.* **2000**, *112*, 9201−9205.
(42) Crivello, J. V.; Narayan, R. *Macromolecules* **1996**, *29*, 439−445.
(43) Crivello, J. V.; Narayan, R. *Macromolecules* **1996**, *29*, 433−438.
(44) Watanabe, N.; Kabasawa, Y.; Takase, Y.; Matsukura, M.; Miyazaki, K.; Ishihara, H.; Kodama, K.; Adachi, H. *J. Med. Chem.* **1998**, *41*, 3367−3372.
(45) Wellmar, U.; Hörnfeldt, A.-B.; Gronowitz, S. *J. Heterocyclic Chem.* **1996**, *33*, 409−414.
(46) Birks, J. B. *Photophysics of Aromatic Molecules*; Wiley-Interscience: New York, 1970.
(47) Saeva, F. D.; Breslin, D. T.; Martic, P. A. *J. Am. Chem. Soc.* **1989**, *111*, 1328−1330.
(48) Saeva, F. D.; Garcia, E.; Martic, P. A. *J. Photochem. Photobiol., A* **1995**, *86*, 149−154.
(49) Rehm, D.; Weller, A. *Isr. J. Chem.* **1970**, *8*, 259.
(50) Berlman, I. B. *Handbook of Fluorescent Spectra of Aromatic Molecules*; 2nd ed.; Academic Press: New York, 1971.
(51) Saeva, F. D.; Breslin, D. T.; Luss, H. R. *J. Am. Chem. Soc.* **1991**, *113*, 5333−5337.
(52) Kampmeier, J. A.; Hoque, A. K. M. M.; Saeva, F. D.; Wedegaertner, D. K.; Thomsen, P.; Ullah, S.; Krake, J.; Lund, T. *J. Am. Chem. Soc.* **2009**, *131*, 10015−10022.
(53) Andrieux, C. P.; Robert, M.; Saeva, F. D.; Saveant, J. M. *J. Am. Chem. Soc.* **1994**, *116*, 7864−7871.
(54) Kamada, K.; Ohta, K.; Iwase, Y.; Kondo, K. *Chem. Phys. Lett.* **2003**, *372*, 386−393.
(55) Drobizhev, M.; Karotki, A.; Kruk, M.; Mamardashvili, M. Z.; Rebane, A. *Chem. Phys. Lett.* **2002**, *361*, 504−512.
(56) Drobizhev, M.; Karotki, A.; Kruk, M.; Rebane, A. *Chem. Phys. Lett.* **2002**, *355*, 175−182.
(57) Drobizhev, M.; Stepanenko, Y.; Dzenis, Y.; Karotki, A.; Rebane, A.; Taylor, P. N.; Anderson, H. L. *J. Am. Chem. Soc.* **2004**, *126*, 15352−15353.